ISSN 1064-2269, Journal of Communications Technology and Electronics, 2021, Vol. 66, No. 4, pp. 473–479. © Pleiades Publishing, Inc., 2021.
Russian Text © The Author(s), 2021, published in Radiotekhnika i Elektronika, 2021, Vol. 66, No. 4, pp. 410–416.

PHYSICAL PROCESSES IN ELECTRON DEVICES

Superconducting Structures for Study and Phase Synchronization of Integrated Terahertz Oscillators

P. N. Dmitriev[a, †], A. B. Ermakov[a], N. V. Kinev[a], O. S. Kiselev[a, b], L. V. Filippenko[a], M. Yu. Fominskii[a], and V. P. Koshelets[a, b, *]

[a] *Kotelnikov Institute of Radio Engineering and Electronics, Russian Academy of Sciences, Moscow, 125009 Russia*
[b] *Institute for Physics of Microstructures, Russian Academy of Sciences, Nizhny Novgorod, 603950 Russia*
**e-mail: valery@hitech.cplire.ru*

Received April 28, 2020; revised April 28, 2020; accepted November 12, 2020

Abstract—Superconducting integrated circuits based on high-quality Nb–AlO_x–Nb and Nb–AlN–NbN tunnel junctions, including a harmonic mixer with a high harmonic number, have been developed, optimized, and investigated. Details of the design, manufacturing methods, and specificities of operation of superconducting elements and circuits for the detection and study of terahertz radiation from cryogenic integrated oscillators are presented. The signal of an integral terahertz oscillator was detected, its power was estimated, and the radiation spectrum was measured with a resolution of about 1 Hz. The synchronization of a superconducting oscillator at any frequency in the range 250–750 GHz with a spectral quality higher than 50% has been realized, and the phase noise of the generator in the PLL mode has been measured.

DOI: 10.1134/S1064226921040033

INTRODUCTION

The idea of using superconducting junctions as integrated detectors of terahertz (THz) radiation generated by an oscillator placed on the same substrate seems to be very natural; it was implemented in many experimental studies [1–5]. In intial articles, the effect of radiation from a THz oscillator was detected by changing the current–voltage characteristic (CVC) of the superconducting detector junction; in this case, it is possible not only to detect the presence of radiation, but also to estimate the signal power within the existing models. Moreover, the use of a superconducting tunnel junction as a mixer makes it possible to measure the spectrum of an integrated heterodyne oscillator [3, 5]. The use of harmonic mixers as part of a superconducting integrated receiver (SIR) [6] made it possible to create practical devices for atmospheric monitoring [7] and measuring the emission spectrum of new solid-state oscillators in the THz range [8]. However, the details of the design and specificities of operation of these fundamentally important elements of the integrated receiver have not been described in sufficient detail until now. This article provides a detailed description of the principles of operation of integrated harmonic detectors and mixers and discusses various designs and topologies of such elements and devices, as well as the results of their application as part of integrated receiving systems and the possibility of their use in the creation of newly developed superconducting THz oscillators.

1. DESIGN OF THE INTEGRATED MIXER AND MODELING AND OPTIMIZATION OF ITS PARAMETERS

The role of an integrated receiving element is usually played by a superconductor–insulator–superconductor (SIS) tunnel junction, which, as a rule, is manufactured simultaneously with the THz oscillator. When designing and selecting the parameters of an integrated superconducting mixer, several important factors should be taken into account. First, an SIS junction with a barrier thickness of about 1 nm has high specific capacity C_{sp} (approximately 0.08 pF/μm^2), which leads to a significant shunting of the high-frequency nonlinear impedance of the junction, $R_{HF}(V)$. At frequencies of 300–700 GHz, the real part of the junction impedance is on the order of its normal impedance R_N. Parameter γ characterizing the degree of shunting can be written as follows:

$$\gamma = 2\pi f R_{HF} C_{sp} A, \quad (1)$$

where f is the radiation frequency and A is the junction area. For a normal impedance of the SIS junction of 25 Ω and an area of 1 μm^2, γ = 6.5 at a frequency of 500 GHz; this means that most of the microwave current flows through the capacitance of the junction, $C_J = C_{sp}A$. The parasitic capacitance can be

[†] Deceased.

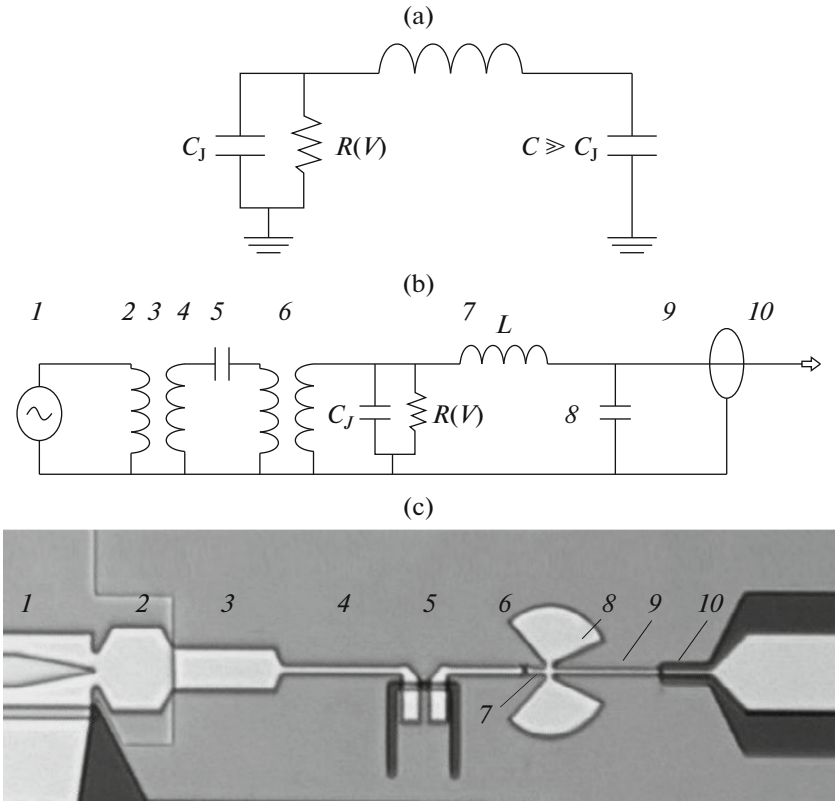

Fig. 1. (a) Equivalent circuit of a SIS junction with elements for detuning the parasitic capacitance at the operating frequency, (b) simplified diagram of the integrated structure, and (c) photograph of the integrated structure for studying the radiation of an oscillator based on a distributed Josephson junction: (*1*) oscillator based on a distributed Josephson junction (only a small fragment of the junction with narrowing is shown); (*2*–*4*) sections of a three-stage impedance transformer; (*5*) DC decoupling; (*6*) one-section impedance transformer; (*7*) SIS junction with inductive section for detuning the capacitance of the SIS junction in the operating frequency range; (*8*) radial sectors forming a capacitance for closing the high-frequency inductive section to the lower electrode; (*9*) quarter-wave microstrip line section for connecting the SIS junction; and (*10*) output coplanar line.

"detuned" at the operating frequency by connecting a small inductance, usually made in the form of a microstrip line segment with a length of several micrometers. The inductance should not shunt the junction at the direct current (DC); to connect the junction only at high frequencies, a "blocking" capacitance is used (Fig. 1a), which can be implemented using broadband radial contactors. It should be noted that detuning range Δf is only a small fraction of the center frequency ($\Delta f \simeq 2f/\gamma$); the higher the junction current density, the smaller γ and the wider the mixer operating range.

The impedance of a SIS structure with detuned capacitance is very low:

$$\mathrm{Re}\,Z_{\mathrm{SIS}} = R_{\mathrm{HF}}/(1+\gamma^2)\,, \qquad (2)$$

and matching to other elements requires the use of impedance transformers. In addition, to provide independent power supply of the oscillator and mixer, DC decoupling of these elements that will not interfere with the passage of the high frequency signal from the generator to the mixer is required. It should also be taken into account that the output impedance of the oscillator is of fractions of an Ohm, which necessitates the use of a multi-section impedance transformer for matching to the decoupling circuit and connecting to the mixer.

Figure 1b shows a simplified diagram of the structure for studying the radiation of the THz oscillator, and Fig. 1c shows a photograph of an experimental integrated structure with a superconducting heterodyne oscillator (SHO) based on a distributed Josephson junction. Figure 1c shows a specific version of the SHO, but the structure can be used to study any other cryogenic thin-film oscillator. This paper presents the results of study of integrated circuits based on Nb–AlO_x–Nb and Nb–AlN–NbN tunnel structures. The technology for manufacturing superconducting integrated structures based on high-quality tunnel junctions was developed and optimized at the Kotelnikov Institute of Radio Engineering and Electronics, Russian Academy of Sciences (IRE RAS) [9–11]; this technology was tested while manufacturing low-noise receivers in the THz range for radio astronomy and integrated receivers for atmospheric monitoring and

laboratory applications [7, 12–14]. The main elements of the matching circuits are made in the form of sections of microstrip lines based on niobium films; the insulator was a 400-nm-thick silicon dioxide (SiO_2) layer (in the first section of the transformer, the thickness of SiO_2 was 200 nm).

The CVC of the Nb–AlO_x–Nb mixing tunnel junction with an area of 1.4 μm^2 is shown in Fig. 2a (curve *A*). The normal impedance of the junction is 20 Ω, the ratio of the impedance under the gap to the normal impedance (quality parameter) is about 30, and the total energy gap is $V_g = 2.8$ mV. The capacitance of the tunnel junction is detuned in a wide frequency band, which makes it possible to detect radiation from 400 to 700 GHz (see Fig. 2a). The figure clearly shows quasiparticle current steps caused by stimulated electron tunneling under the action of photons. The steps grow from the gap singularity, and their position is determined by expression

$$V = V_g \pm hf/e, \quad (3)$$

where h is the Planck constant, f is the radiation frequency, and e is the electron charge. By measuring the pump current at a step voltage, one can estimate the radiation power reaching the detector (Fig. 2b). The power released in the junction can be estimated by comparing the experiment with calculations within the Tucker and Feldman theory [15]; the calculations were carried out with a model CVC (see, e.g., [16]). The model CVC fully coincides with the experimental dependence (compare curves *A* in Figs. 2c and 2a). Figure 2c also shows the calculated curves for two values of high-frequency voltage V_{HF} for a pumping frequency of 600 GHz. The main parameter for describing quasiparticle current steps is the normalized high-frequency voltage:

$$\alpha = eV_{HF}/hf\ . \quad (4)$$

The figure shows calculated CVCs for $\alpha = 1$ and 2; note that the first value corresponds to the optimal pumping level for the operation of low-noise SIS mixers. It can be seen that the calculated dependences describe the experimental curves fairly well (Fig. 2b); small deviations are caused by the need to take into account the effect of the external electrodynamic system, which depends on the frequency. In the experimental curves at voltages of about 1.2 and 2.4 mV, we see Josephson current steps ($V_J = nhf/2e$); these steps make it possible to determine with sufficient accuracy the radiation frequency in the case of incomplete suppression of the critical current.

For an accurate estimation of the power released in the junction, it is necessary to know the real part of the high-frequency impedance of the SIS junction, $\mathrm{Re}Z_{HF}$. Its value can be calculated within the model [15], but, in a real situation, it is necessary to take into account the impedance of the external electrodynamic system. In order to estimate the power of an SHO, it is also necessary to take into account its matching to the receiver. These calculations require taking into account the behavior of superconducting films at a high frequency and knowing the parameters of all structures. Figure 3a shows the results of calculating the matching of the SHO to the SIS junction, θ, for

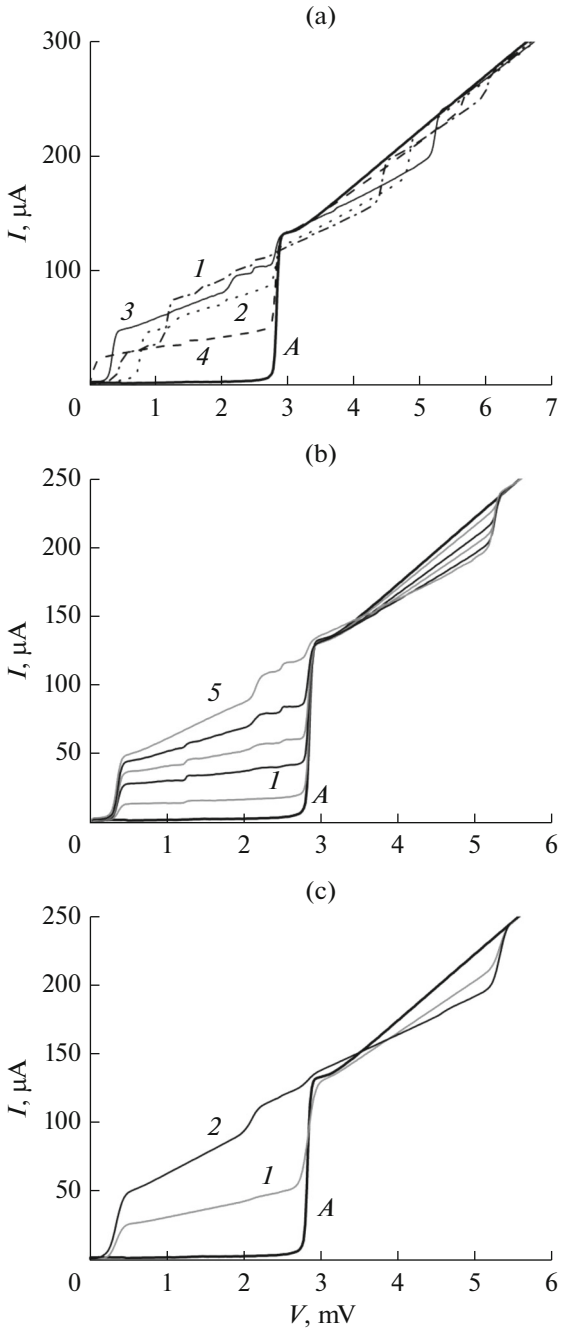

Fig. 2. (a) CVC of the Nb–AlO_x–Nb tunnel junction with an area of 1.4 μm^2 under the action of SHO's power at frequencies of (*1*) 400, (*2*) 500, (*3*) 600, and (*4*) 700 GHz; (b) CVC of a SIS junction at different values of the SHO's power at a frequency of 600 GHz; model CVC at $\alpha = 0$, (*1*) 1 and (*2*) 2; in all figures, *A* is the autonomous CVC.

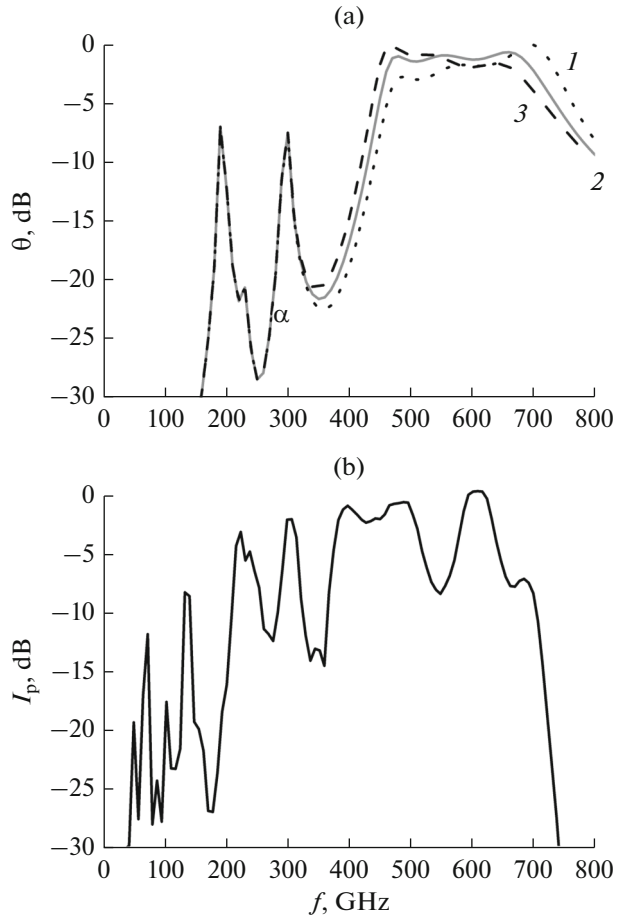

Fig. 3. (a) Calculated impedance matching of the SHO and SIS junction θ vs. frequency for the circuit shown in Fig. 1 for A = (*1*) 1.1 (1), (*2*) 1.4, and (*3*) 1.7; (b) experimental dependence of the pump current of the SIS junction I_p at a voltage of 2.5 mV on the SHO frequency (the pump current is normalized to the maximum value at a frequency of 600 GHz).

three values of the junction area. Figure 3b shows the pump current of the SIS junction, measured at a voltage of 2.5 mV, as a function of the SHO frequency. The pump current of the SIS junction characterizes the power of the received HF signal, which, in turn, is determined by the matching of circuit elements. It can be seen that the experimental dependence is in good agreement with the calculation; the dip at a frequency of 550 GHz is apparently caused by resonances in the structure, which were not taken into account in the model, and an incomplete correspondence of the measured parameters of the structure to the values used in the model. It should be noted that the calculation used the model of a perfect conductor and did not take into account the increase in losses in niobium films at frequencies above the energy gap (about 720 GHz). The excess of the measured values of the pump current over the model results at frequencies below 400 GHz is due to the fact that the radiation of the SHO contains the second and third harmonics. At the SHO fundamental frequency of 300 GHz, at which the matching is small, the second harmonic at 600 GHz is well matched, which leads to the pumping of the mixer; it is detected as the effect at the fundamental frequency of 300 GHz. Thus, a properly designed circuit based on a superconducting junction makes it possible to measure the THz signal of the SHO and estimate its frequency and power.

2. INTEGRATED HARMONIC MIXER FOR MEASURING THE SPECTRA OF THE SHO AND ITS PHASE SYNCHRONIZATION

The integrated structure described above can be used not only for detecting a signal of a SHO, but also for measuring its radiation spectrum, as well as for stabilizing the SHO frequency [5, 17–21]. A schematic diagram of such an experiment is shown in Fig. 4. The main element is the SIS tunnel junction, which is used as a harmonic mixer with a high harmonic number [22–24]. The signal from the reference synthesizer (10), f_{syn}, with a frequency of about 20 GHz is fed through directional coupler *1* to the SIS junction in which the nth harmonic of the synthesizer signal is

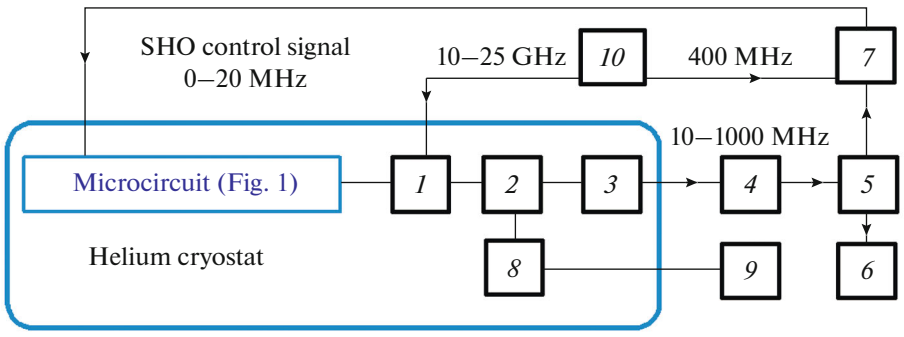

Fig. 4. Block diagram of the system for measuring the radiation spectra of the SHO and its phase synchronization: (*1*) directional coupler for input of the reference signal in the range 10–25 GHz, (*2*) multiplexer of IF and DC signals, (*3*) cryogenic HEMT amplifier for the range 10–1000 MHz, (*4*) additional amplifier, (*5*) splitter, (*6*) spectrum analyzer, (*7*) phase-locked loop with frequency detector, (*8*) cryogenic filters for harmonic mixer, (*9*) bias and measurement unit for harmonic mixer, and (*10*) synthesizer.

mixed with the SHO signal with a frequency f_{SHO}. The difference signal at intermediate frequency f_{IF} (about 1 GHz),

$$f_{IF} = \pm(f_{SHO} - nf_{syn}) \quad (5)$$

is fed to cryogenic amplifier *3* based on a high electron mobility transistor (HEMT) (noise temperature of about 5 K, gain of 30 dB), is output from the cryostat, and goes to additional amplifier *4* (adjustable gain of 40–60 dB). Next, the converted signal is branched to spectrum analyzer *6* to record spectra and to a phase-locked loop (PLL) with additional frequency detector *7*. The frequency detector with a regulation bandwidth of about 10 kHz stabilizes the frequency, eliminating low-frequency interference and temperature drifts (see Fig. 5a). The figure shows the frequency dependence of the output IF signal $P_{IF}f_{IF}$; we can see an autonomous line of SHO radiation based on the Nb–AlO_x–Nb distributed tunnel junction, linewidth $\delta f = 1$ MHz is determined by the resolution of the spectrum analyzer, and the signal-to-noise ratio is 45 dB. The real linewidth is 0.5 MHz (see Fig. 5b), where the same line was measured with a resolution of 100 kHz. When using the PLL system, the incoming signal is compared with the 400 MHz reference signal from the synthesizer, and the phase error signal is fed to the SHO to stabilize its frequency. The result is shown in Fig. 5c; the ratio of the signal in the central peak to the total power, the so-called spectral quality (SQ), is 97.5%. The regulation bandwidth of the PLL system is about 17 MHz; it is determined by the length of the cables from the harmonic mixer to the PLL and back to the SHO. It should be noted that the ratio of this value to the autonomous width of the SHO generation line determines the final SQ: the wider the line, the lower SQ can be obtained [25].

The magnitude of the relative phase noise of the SHO in the PLL mode, Ψ, as a function of detuning Δf from center frequency f is shown in Fig. 6 (curve *1*). This noise was measured relative to a reference synthesizer; in order to obtain the absolute phase noise, it is necessary to add the noise of the reference synthesizer (curve *2*), multiplied by the square of the harmonic number ($n = 20$); the magnitude of the absolute phase noise is represented by curve *4*.

It should be noted that the technique developed makes it possible to measure the radiation spectrum of the oscillator and provide the PLL mode even at a low level of SHO power reaching the harmonic mixer. Figure 7 shows the current of the harmonic mixer, induced by the SHO at a frequency of 670 GHz (without feeding a synthesizer signal), and the resulting SQ versus of the SHO bias current (this quantity determines the power radiated by the SHO). It can be seen from the figure that the limiting value of the SQ (determined by the SHO parameters) can be realized even at a low power of the incoming signal (the SHO bias current is 14 mA). This power produces only a small induced current in the harmonic mixer (4% of the maximum pump current). In addition, the SIS junction has two coexisting convertion modes. The first one, which is now widely used, is the quasiparticle mode, based on the effect of stimulated tunneling of electrons under the action of photons [15, 22]; in this case, the critical current is suppressed by an external magnetic field, and, therefore, it is possible to obtain noise temperatures close to quantum limit hf/k_B

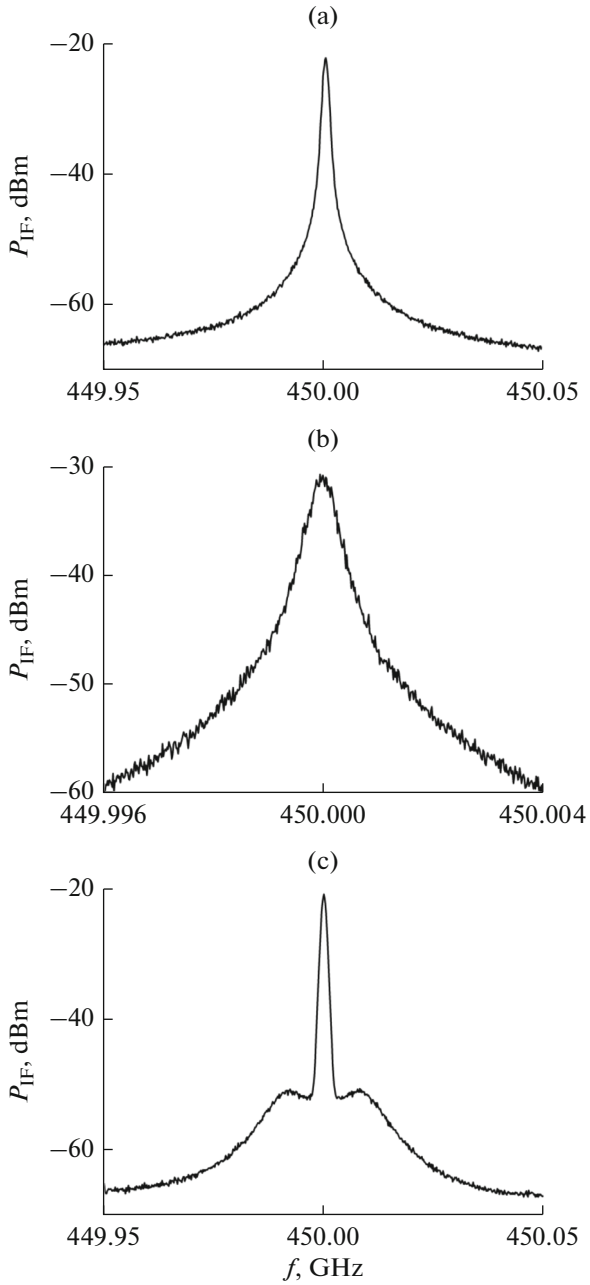

Fig. 5. SHO radiation spectrum at a frequency of 450 GHz, measured using a harmonic mixer: in the frequency stabilization mode in a spectrum analyzer resolution bandwidth of (a) 1 and (b) 100 MHz and (c) in the phase stabilization mode with a resolution of 1 MHz.

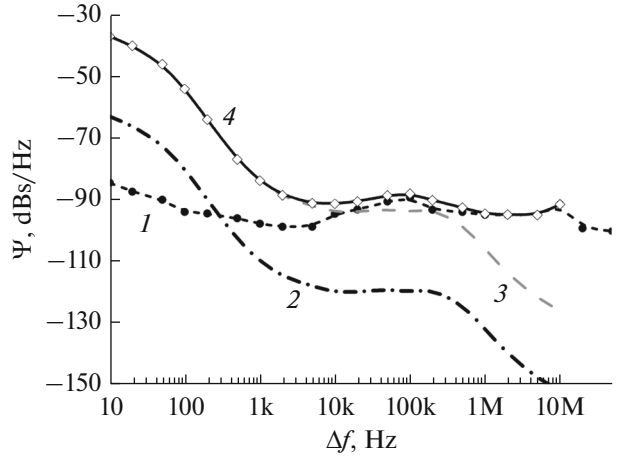

Fig. 6. (*1*) SHO phase noise Ψ at a frequency of 450 GHz vs. detuning Δf from carrier frequency f (curve *1*); (*2*) phase noise of the reference synthesizer at the fundamental frequency of 22.48 GHz and (*3*) at the 20th harmonic; and (*4*) the total (absolute) phase noise of such an oscillator in the PLL mode with allowance for the contribution of synthesizer noise.

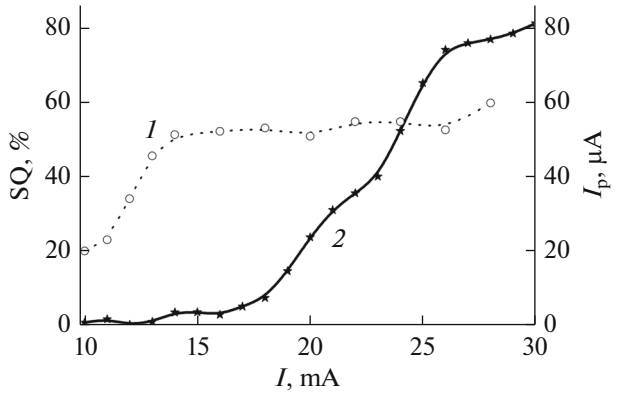

Fig. 7. (*1*) Spectral quality of the SHO in the PLL mode at 670 GHz and (*2*) the corresponding pump current of the harmonic mixer vs. oscillator's supply current.

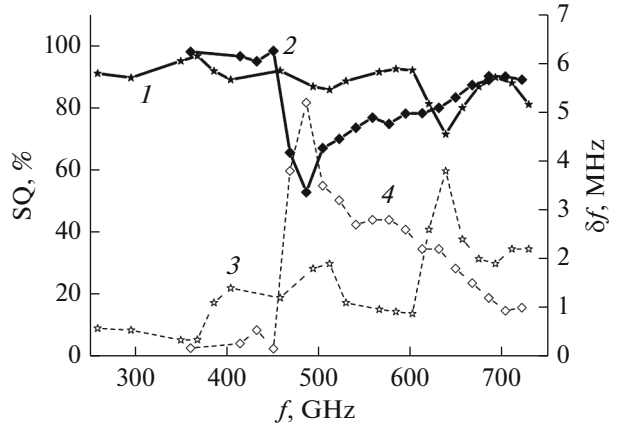

Fig. 8. (*3*, *4*) SHO autonomous radiation linewidth δf and (*1*, *2*) the resulting spectral quality (SQ) of the SHO in the PLL mode vs. oscillator frequency: for SHO based on (*1*, *3*) Nb–AlN–NbN and (*2*, *4*) Nb–AlO_x–Nb structures.

[7, 14, 15]. The second, the Josephson mode using the nonlinearity of the superconducting current, makes it possible to obtain lower convertion losses, but is characterized by a higher noise level. These two modes were studied and compared in [23, 24], which showed that, when operating in the Josephson mixer mode with a high harmonic number, the presence of a powerful heterodyne signal makes it possible to realize close values of the signal-to-noise ratios for both cases, while the output signal of the Josephson mixer exceeds by 1–2 orders of magnitude the quasiparticle signal, which is important for efficient operation of the PLL system.

The technique developed and the use of a mixed convertion mode (without suppressing the Josephson current) make it possible to measure the radiation line of cryogenic oscillators in a very wide frequency range, using only one integrated harmonic mixer. An example of such measurements at frequencies from 250 to 750 GHz for two types of SHO is shown in Fig. 8, which compares the results for the best oscillators based on distributed Nb–AlO_x–Nb and Nb–AlN–NbN junctions [25]. Due to the Josephson self-pumping effect [26], at voltages $V_g/3$, the damping in the SHO sharply increases, which leads to an increase in linewidth δf and a reduction in the spectral quality in the transition voltage region slightly above $V_g/3$. For Nb–AlO_x–Nb junctions, the transition occurs at a frequency of 450 GHz, and, for Nb–AlN–NbN junctions, at 600 GHz. The measurements performed made it possible to develop and successfully test integrated receivers for practical applications with required frequency characteristics [6–8, 25].

CONCLUSIONS

In this paper, we have given a detailed description of the principles of operation of integrated harmonic detectors and mixers and considered various designs and topologies of such elements, as well as the results of their application as part of integrated receivers. It has been shown that, on the basis of the approach developed, it is possible to measure the spectrum of cryogenic heterodyne generators in the range of 250–750 GHz, as well as to provide their phase locking with a spectral quality of 50 to 98% in the entire frequency range. The design studies have made it possible to create integrated receivers for monitoring Earth's atmosphere and laboratory applications [7, 8, 25]. Similar approaches can be used to study newly developed superconducting terahertz oscillators [27] designed to study new strategies for mutual synchronization of large arrays of Josephson junctions.

FUNDING

This study was supported by the Russian Science Foundation (project no. 20-42-04415). The tunnel junctions

were manufactured at the IRE RAS as part of a state assignment and using Unique Scientific Unit No. 352529.

REFERENCES

1. T. Nagatsuma, K. Enpuku, F. Irie, and K. Yoshida, J. Appl. Phys. **54**, 3302 (1983).
2. K. L. Wan, A. K. Jain, and J. E. Lukens, IEEE Trans. Magn. **25**, 1076 (1989).
3. Y. M. Zhang, D. Winkler, and T. Claeson, Appl. Phys. Lett. **62**, 3195 (1993).
4. V. P. Koshelets, A. V. Shchukin, S. V. Shitov, and L. V. Filippenko, IEEE Trans. Appl. Supercond. **3** (1), 2524 (1993).
5. V. P. Koshelets, S. V. Shitov, A. V. Shchukin, et al., Appl. Phys. Lett. **69**, 699 (1996).
6. V. P. Koshelets and S. V. Shitov, Supercond. Sci. Technol. **13** (5), R53 (2000).
7. G. de Lange, D. Boersma, J. Dercksen, et al., Supercond. Sci. Technol. **23**, 045016 (2010).
8. M. Li, J. Yuan, N. Kinev, et al., Phys. Rev. B **86**, 060505 (2012).
9. V. P. Koshelets, S. A. Kovtonyuk, I. L. Serpuchenko, et al., IEEE Trans. Magn. **27**, 3141 (1991).
10. L. V. Filippenko, S. V. Shitov, P. N. Dmitriev, et al., IEEE Trans. Appl. Supercond. **11**, 816 (2001).
11. P. N. Dmitriev, I. L. Lapitskaya, L. V. Filippenko, et al., IEEE Trans. Appl. Supercond. **13**, 107 (2003).
12. V. P. Koshelets, A. B. Ermakov, L. V. Filippenko, et al., IEEE Trans. Appl. Supercond. **17**, 336 (2007).
13. V. P. Koshelets, P. N. Dmitriev, M. I. Faley, et al., IEEE Trans. Terahertz Sci. Technol. **5**, 687 (2015).
14. K. I. Rudakov, P. N. Dmitriev, A. M. Baryshev, et al., Izv. Vyssh. Uchebn. Zaved., Radiofiz. **62**, 613 (2019).
15. J. R. Tucker and M. J. Feldman, Rev. Mod. Phys. **57**, 1055 (1985).
16. S. V. Shitov, *Integrated Devices on Superconducting Tunnel Junctions for Millimeter and Submillimeter Wave Receivers*, Doctoral (Phys. Math.) Dissertation (IRE im. V.A. Kotelnikova RAN, Moscow, 2003).
17. V. P. Koshelets, S. V. Shitov, P. N. Dmitriev, et al., Physica C **367**, 249 (2002).
18. V. P. Koshelets, S. V. Shitov, A. V. Shchukin, L. V. Filippenko, P. N. Dmitriev, V. L. Vaks, J. Mygind, A. M. Baryshev, W. Luinge, and H. Golstein, IEEE Transactions on Applied Superconductivity **9**, 4133 (1999).
19. V. P. Koshelets, S. V. Shitov, L. V. Filippenko, et al., Rev. Sci. Instrum. **71**, 289 (2000).
20. N. V. Kinev, K. I. Rudakov, L. V. Filippenko, et al., J. Appl. Phys. **125**, 151603 (2019).
21. N. V. Kinev, K. I. Rudakov, L. V. Filippenko, et al., IEEE Trans. Terahertz Sci. Technol. **9**, 557 (2019).
22. K. V. Kalashnikov, A. V. Khudchenko, A. B. Baryshev, and V. P. Koshelets, J. Commun. Technol. Electron. **56**, 699 (2011).
23. K. V. Kalashnikov, A. A. Artanov, L. V. Filippenko, and V. P. Koshelets, Phys. Solid State **58**, 2191 (2016).
24. K. V. Kalashnikov, A. A. Artanov, G. de Lange, and V. P. Koshelets, IEEE Trans. Appl. Supercond. **28**, 2400105 (2018).
25. P. N. Dmitriev, L. V. Filippenko, and V. P. Koshelets, *Josephson Junctions. History, Devices, and Applications*, Ed. by E. Wolf, G. Arnold, M. Gurvitch, and J. Zasadzinski, (CRC Press, Boca Raton, FL, 2017), p. 185.
26. V. P. Koshelets, S. V. Shitov, A. V. Shchukin, et al., Phys. Rev. B **56**, 5572 (1997).
27. M. A. Galin, E. A. Borodianskyi, V. V. Kurin, et al., Phys. Rev. Appl. **9**, 054032 (2018).

Translated by E. Chernokozhin